Research Article Vol. 10, No. 1 / January 2023 / Optica 53

Tunable THz flat zone plate based on stretchable single-walled carbon nanotube thin film

Gleb M. Katyba,[1,2,3,*] Nikita I. Raginov,[4] Eldar M. Khabushev,[4] Vladislav A. Zhelnov,[2] Andrei Gorodetsky,[5] Davit A. Ghazaryan,[3] Mikhail S. Mironov,[3,6] Dmitriy V. Krasnikov,[4] Yuri G. Gladush,[4] James Lloyd-Hughes,[7] Albert G. Nasibulin,[4] Aleksey V. Arsenin,[3,6] Valentyn S. Volkov,[3,6] Kirill I. Zaytsev,[2] and Maria G. Burdanova[1,3,8]

[1]Institute of Solid State Physics of the Russian Academy of Sciences, 2 Academician Osipyan str., Chernogolovka, 142432, Russia
[2]Prokhorov General Physics Institute of the Russian Academy of Sciences, 38 Vavilova str., Moscow, 119991, Russia
[3]Center for Photonics and 2D Materials, Moscow Institute of Physics and Technology, 9 Institutskiy Lane, Dolgoprudny, 141701, Russia
[4]Skolkovo Institute of Science and Technology, 3 Nobel str., Moscow, 121205, Russia
[5]University of Birmingham, Birmingham, B15 2TT, UK
[6]Emerging Technologies Research Center, XPANCEO, Dubai, United Arab Emirates
[7]Department of Physics, University of Warwick, Gibbet Hill Road, Coventry, CV4 7AL, UK
[8]e-mail: burdanova.mg@mipt.ru
*Corresponding author: katyba_gm@issp.ac.ru

Received 13 September 2022; revised 15 November 2022; accepted 15 November 2022; published 6 January 2023

Tunable optoelectronics have attracted a lot of attention in recent years because of their variety of applications in next-generation devices. Among the potential uses for tuning optical elements, those allowing consistent parameter control stand out. We present an approach for the creation of mechanically tunable zone plate lenses in the THz range. Our devices comprise single-walled carbon nanotube (SWCNT) thin films of predetermined design integrated with stretchable polymer films. These offer high-performance and *in situ* tunability of focal length up to 50%. We studied the focusing properties of our lenses using the backward-wave oscillator THz imaging technique, supported by numerical simulations based on the finite element frequency domain method. Our approach may further enable the integration of SWCNT films into photonic and optoelectronic applications and could be of use for the creation of a variety of flexible and stretchable THz optical elements.

https://doi.org/10.1364/OPTICA.475385

1. INTRODUCTION

Applications dealing with THz waves became one of the emerging fields of interest in science and technology due to their extraordinary properties, such as non-destructive nature, high spatial resolution, penetration depth, and high sensitivity. Adaptive beamforming [1,2], biophotonics [3], imaging [4,5], and high-speed indoor communication [6] play important roles in the development of THz technologies. Many of those call for stretchable, flexible, lightweight solutions unavailable for bulky and rigid conventional solid-state devices.

Single-walled carbon nanotube (SWCNT) films demonstrate high absorption in the THz spectral range and offer exceptionally low thicknesses [7–9] and strain rates [10]. Recent progress in their synthesis allows the production of large area, uniform, and chemically free films through the chemical vapor deposition (CVD) technique [11]. Such films could be easily transferred onto the desired substrate [12]. SWCNT films exhibit high intrinsic carrier mobility and high conductivity and show potential for the development of detectors [13], sources [14], and modulators [15] in the THz spectral range. Advancements in polymer technologies boosted flexible and stretchable optoelectronics enabling the design and fabrication of such high-frequency devices. In electronics, flexible and stretchable devices based on SWCNT films integrated with polymer substrates have been widely implemented and studied [16,17]; however, only a few studies report on THz devices [18,19]. THz spectral range devices with controllable parameters are of significant interest for the development of THz technologies.

THz lenses play an essential role in a variety of applications, such as spectroscopy [20,21], communication [22], imaging [23], and standoff detection [24] systems. Those are usually made from polymer or crystalline materials, and therefore have fixed focal lengths. Notably, variable-focus lenses were developed a long time ago for the visible range [25,26]. In contrast, only several studies report on the modification of the focal length of THz lenses [27–29]. Chen *et al*. presented a THz plasmonic lens based on InSb micropatterns and controlled by temperature [29]. Scherger *et al*.

demonstrated a lens made of medical white oil injected between two elastic polymer foils [27]. Wichmann *et al*. used a mixture of polymers to tune the refractive index, and hence the parameters of the lens [30]. The fabrication procedures of these lenses, though very promising due to their high performance, rely on complicated design and operating principles.

This research aims to shed light on an alternative type of lens based on planar optical elements, namely, stretchable Fresnel zone plates. For the first time, this stretchable optical element was designed for THz frequencies. Our optical elements with alternating transparent and opaque rings within zone plates can be of use in a variety of modern THz optoelectronic applications, such as focusing optical elements [31–33], lens-antennas [34,35], and nonlinear metasurface sources [36]. Furthermore, by integrating conductive SWCNT films within opaque rings of stretchable polymer-based plates, we demonstrate convenient control over the basic properties of our lenses. In this case, radial stretching of the zone plate allows varying the focal point position and the focal spot dimensions of our lenses. It is interesting that a similar approach was employed for different frequency ranges in [37,38], when Fresnel zone plates with variable focuses based on different stretchable materials were proposed. However, the degree of tunability is not high. In this paper, we translate this concept to the rapidly developed and industry-important THz range, where the problem of designing varifocal lenses appears to be even more important, as well as study systematically the focusing properties of a pilot stretchable THz zone plate. The observed tunable focusing properties are in good agreement with our numerical and analytical modeling results. During the stretching experiment, a 50% change of the focal point position was achieved with a 20% increase in the outer radius of our lens.

2. DESIGN AND FABRICATION

SWCNTs were synthesized by the aerosol (floating catalyst) CVD method [39] based on CO decomposition via the Boudouard reaction on the surface of Fe-based catalyst particles. The Fresnel lens configuration presented here utilizes SWCNT films as opaque areas, and 0.2-mm-thick elastomer (Silpuran, Wacker), as a transparent stretchable substrate. The main fabrication steps are schematically depicted in Fig. 1. In the first step, a nitrocellulose filter (HAWP, Merck Millipore with 0.45 μm pore size) was put on a copper stencil [Fig. 1(a), top left]. In the second step, a silicone (ABRO RTV Silicone Gasket Maker) sealant was deposited on a nitrocellulose filter on the area free of the copper stencil [Fig. 1(b), top right]; after that, the copper stencil was accurately removed to prevent silicone sticking to the stencil. The sealant easily wets pores of the hydrophilic filter while the subsequent silicone formation clogs the particular air path. The resulted silicone pattern has the same thickness as copper foil (200 μm). In the next step, SWCNT aerosol was deposited on an area of the nitrocellulose filter free of the sealant to form a thin CNT film with a pattern similar to the copper stencil geometry [Fig. 1(c), bottom left]. Finally, the obtained film was dry-transferred [40] onto a stretchable substrate [Fig. 1(d), bottom right]. We design a lens with adaptive size and highly sensitive focus tuning, as schematically depicted in Fig. 1(e). The SWCNT film thickness is a few times smaller than the considered THz wavelength, but much larger than the THz wave skin depth due to high conductivity.

In Figs. 2(a) and 2(b), a copper stencil and as-fabricated zone plate are presented. The collected films consist of individual SWCNTs featuring disordered spatial orientation, evident from a scanning electron microscope (SEM) image [Fig. 2(d)]. SWCNTs have a mean diameter of around 1.9 nm obtained from the positions of M_{11}, S_{22}, and S_{11} excitonic peaks from UV-VIS-NIR spectra [see Fig. 2(e)] using the Kataura plot [41]. Figure 2(f) shows the Raman spectrum of SWCNT film. The high quality (low number of defects) of the samples is evident from the low D mode intensity in comparison with the G band ($I_G/I_D > 100$) [42]. The films have a conductivity of c.a. 600 S/cm and considerable elasticity [43].

The initial copper-based pattern for SWCNT zone plate fabrication [see Fig. 2(a)] consists of 10 zones. Although higher zone numbers might provide a sharper focus by suppressing a higher-order focus, the formation of smaller pitches for the high-order zones is challenging due to the spatial resolution of direct SWCNT deposition. Notably, the copper stencil cannot be used as a mask to pattern SWCNT film with predetermined geometry and good quality [see an example of such a low-quality zone plate in Fig. 2(c)]. This is due to the high ability of the aerosol to seep through the copper mask. Therefore, for SWCNT-based zone plate fabrication, we used a nitrocellulose filter with a silicone sealant pattern deposited onto it. The stretch system was reproduced by the authors of [44]. An increase in the radius of the zone plate (and the radius of its zones) will increase the focal length. The working principle of our zone plate is depicted in Fig. 2(e). A full stretch up to 21% is performed, although it is possible to stretch the elastomer with SWCNT film up to $\Delta R_n/R_n = 40\%$ without significant changing of the relative resistance [43]. Notably, stretching was limited to 20% to avoid the irreversible modification of lenses.

Before the lens was tested, several stretching circles were performed to avoid the effects caused by the deformation of both

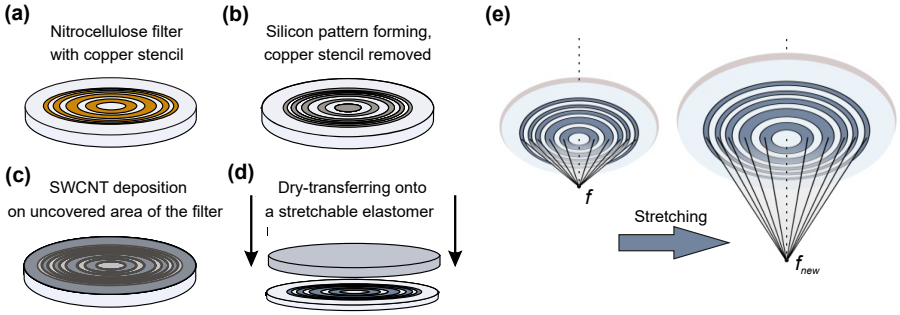

Fig. 1. Schematic illustration of the stretchable zone plates based on SWCNTs. (a)–(d) Fabrication procedure. A nitro-cellulose filtered SWCNT is deposed on top of a silicon pattern and transferred onto a stretchable substrate. (e) Operating principle. *In situ* zone plate stretching results in direct focal length tuning: f is the focal point of the undistorted zone plate, and f_{new} is the focal point after stretching.

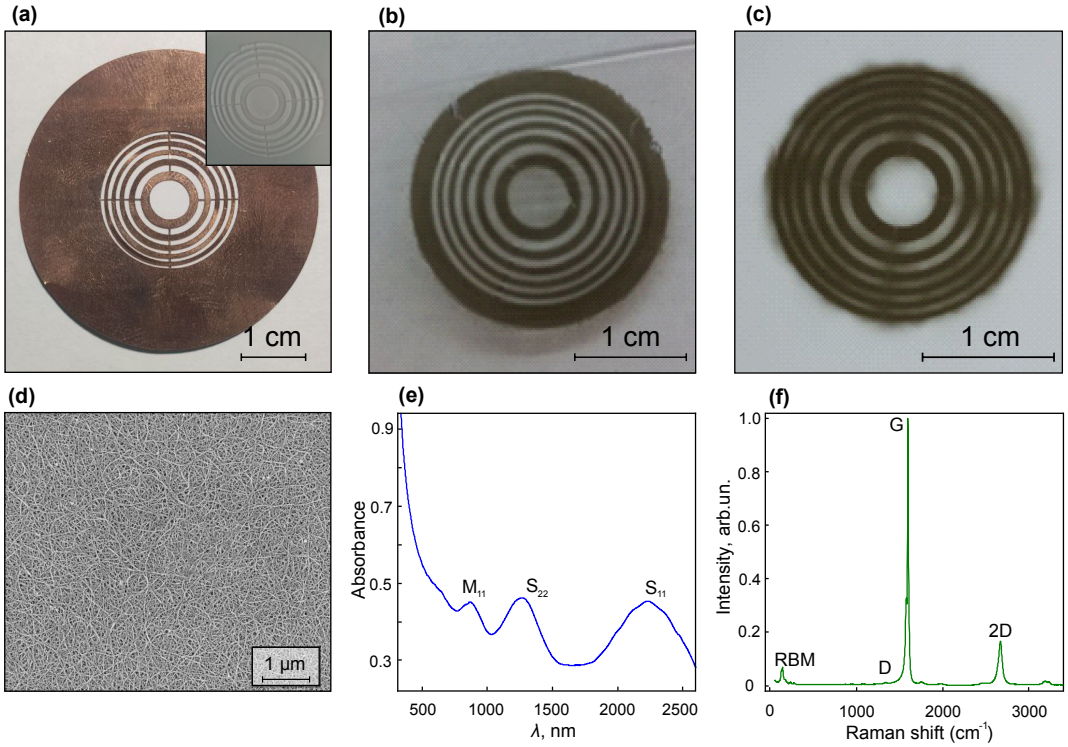

Fig. 2. Fabricated zone plates based on SWCNTs. Optical images of (a) initial patterned mask (copper) and (b) final 10 ring-zone plate (the large outer ring was scraped off later mechanically). In the inset is shown the corresponding silicone pattern on the nitrocellulose filter with inverse geometry. (c) Low-quality zone plate fabricated using only copper stencil without sealant pattern on the filter. (d) SEM image of the SWCNT film; SWCNTs are randomly oriented. (e) UV-VIS-NIR spectrum of the SWCNT film. M_{11}, S_{11}, and S_{22} denote metallic and semiconducting SWCNT transitions, respectively. (f) Raman spectrum of SWCNT film. Legends denote the radial breathing mode (RBM), tangential modes (G-band), disorder-induced modes (D-band), and 2D band of SWCNTs.

SWCNT films and elastomer [43]. As a result, in the current experimental studies, relatively high repeatability was obtained after multiple bending.

3. MEASUREMENT RESULTS

Figure 3 presents the THz imaging system used in the experimental part of SWCNT zone plate characterization; see details in Section 7. A backward-wave oscillator (BWO) was chosen as a source of radiation [45]. The zone plate was clumped on the customized stretching device [see Fig. 3(a)] and placed at the homogenizing part of the setup in front of the detector [Fig. 3(b)]. As a result, 2D cross sections of the THz field intensity $I(\mathbf{r})$ near the zone plate focal spot (here $\mathbf{r}$ is a 3D radius vector) for different stretchings were registered using the translation system [Fig. 3(c)] and are shown in the insets of Figs. 4(a)–4(f). The yoz plane was

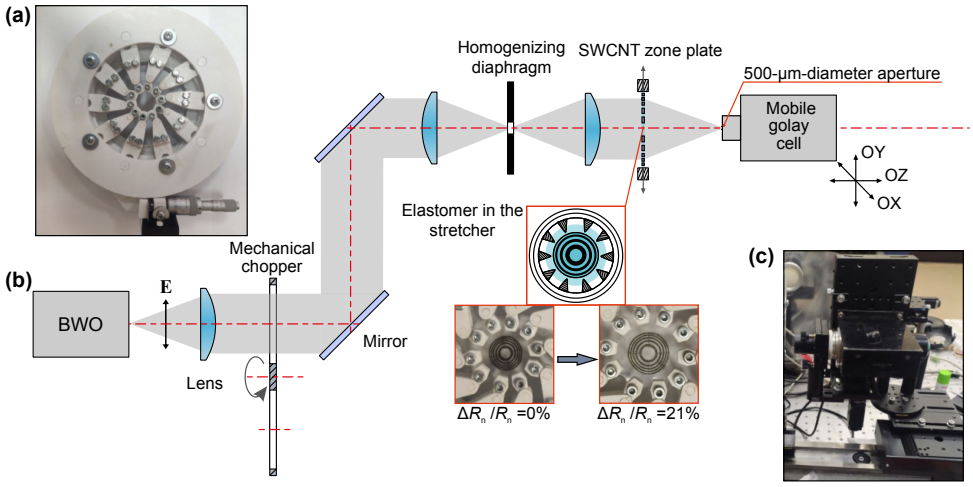

Fig. 3. Experimental THz imaging system for SWCNT-based zone plate characterization. (a) Photo of the stretchable SWCNT zone plate placed in the stretching device. (b) Schematic illustration of the imaging system. (c) Photo of the 500 μm diameter aperture Golay cell mounted in the 2D planar translational system.

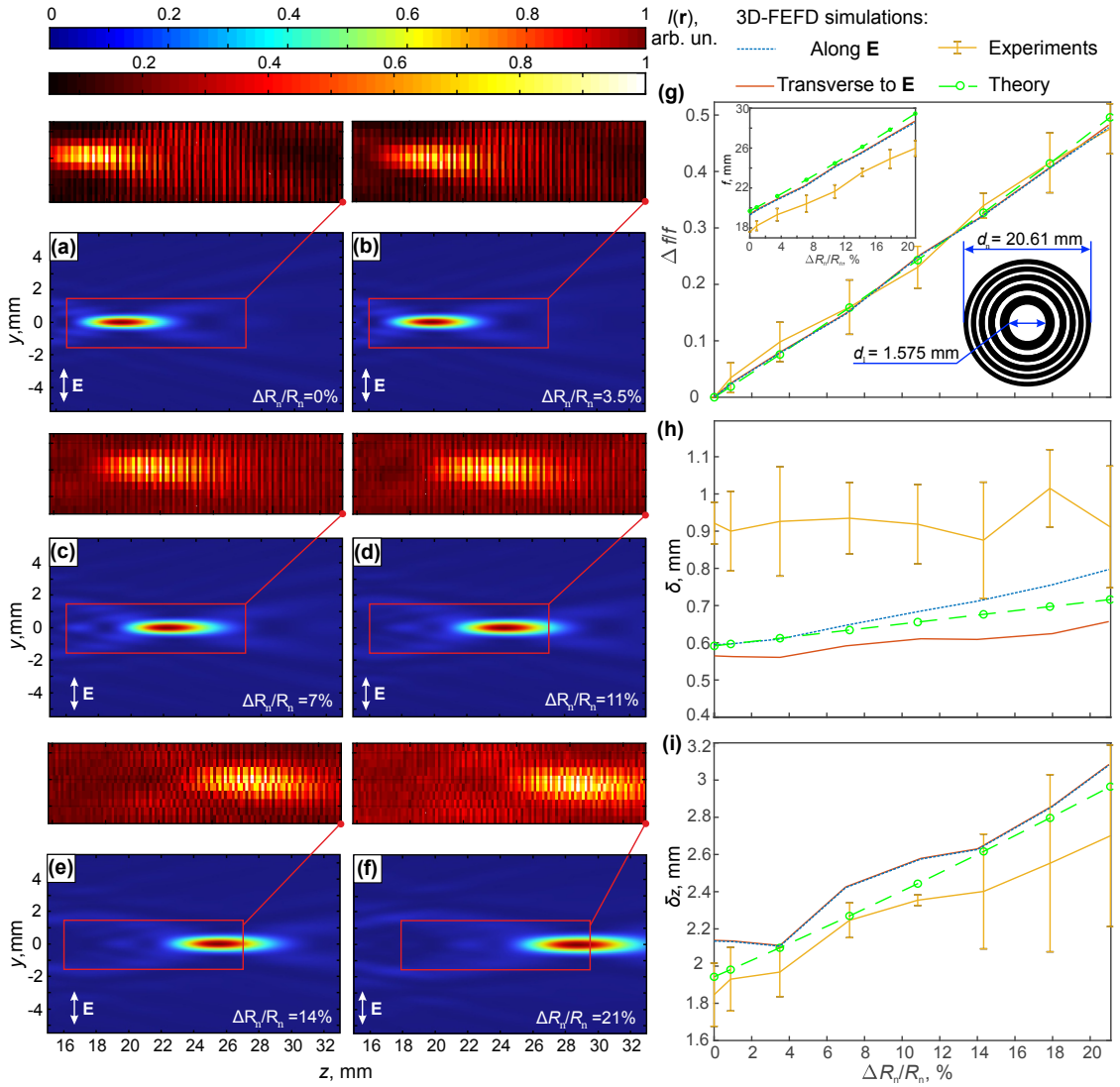

Fig. 4. THz beam focusing by the stretchable zone plate based on SWCNTs. (a)–(f)Axial cross sections of the THz beam caustic $I(y, z)$ at various stretching degrees: relative radius $\Delta R_n/R_n = 0$, 3.5, 7, 11, 14 and 21%. The scanning fields are marked by red rectangles. The insets show corresponding experimental images of THz fields $I(y, z)$ behind the zone plate. (g) Relative change of the focal length $\Delta f/f$. Experimentally obtained results are shown in yellow, analytical estimations are shown in green, and numerically computed results are shown in blue and red for the two perpendicular directions, throughout (g)–(i). The insets demonstrate (left) focus dependence on stretching, and (right) schematic illustration of the undistorted zone plate. (h) Spatial resolution and (i) depth of field.

chosen as an image plane, origin (0,0,0), which corresponds to the point in the center of the optical element. Scanning steps along z-axis and y-axis directions were $\Delta z = 0.1$ mm and $\Delta y = 0.3$ mm, respectively. The experimentally measured focus position was increased monotonically in agreement with simulations [see the inset of Fig. 4(g)]. As expected, smaller stretching results in a better capability for radiation focusing in contrast to stronger stretching. It can be attributed to a small-to-moderate irregularity during zone plate stretching. For example, it could appear due to the surface deviation in rectilinear projection as a pincushion type radial distortion (by parity of reasoning with the same optical aberration [46]) or radius change in different directions caused by imperfections of the stretching device manufacturing. Another reason could be the SWCNT film conductivity changing [19] under strong stretching. Thin cracks that can be seen in the inset of Fig. 3(b) appear on the SWCNT film and could influence the optical properties of the zone plate. Finally, it is important to note that the lens stretching is accompanied by the rotation of the lens due to the operating principle of the stretching device. During zone plate stretching, the optical element can be somewhat shifted from the BWO beam optical axis in the lateral directions, which is due to the applied construction of the stretching device. However, the maximal displacement of the zone plate is less than 0.5–0.7 mm, which is close to the output wavelength of our BWO emitter, as well as comparable to or smaller than dimensions of the THz beam caustic formed by the zone plate at the focal plane. Displacement might cause uncertainty in the experimental estimations of the focal spot positions. In this study, we compensated for this effect (lateral displacements of the beam caustic) manually during the experimental data analysis, while studying the stretchable zone plate performance.

4. SIMULATION RESULTS

A series of numerical quasi-3D simulations of the field transformation by the zone plate with variable dimensions was performed; a detailed description of the simulation method is presented in Section 7. Input frequency was $\nu \simeq 0.592$ THz, which corresponds to the free-space wavelength of $\lambda = 506.66$ μm (this particular wavelength was selected to match a maximum of the BWO outer power). When the radius of the zone plate increases, the focal length and dimensions of the focal spot also increase. The different zone plate outer radius values in simulations correspond to different stretching degrees in the experiment. Figures 4(a)–4(f) demonstrate the simulation distributions of the field intensity $I(y, z)$ near the focal point of the zone plates with different outer zone radii R_n (for the image zoy plane, the oz axis is the optical axis of the simulated element). The zone plate is not shown in this distribution and is located left at $z = 0$. Also, we performed simulations for a perfect infinite plane wave for both longitudinal (in the vector **E** plane) and transverse directions [Figs. 4(a)–4(f) show the intensity distributions only for the first one]. The focal length relative increment $\Delta f/f$ along with the values of spatial resolution δ and depth of field δz for different $\Delta R_n/R_n$ are presented in Figs. 4(g)–4(i) for the two perpendicular directions (parameters δ and δ_z also were fitted with the Gaussian function in both the simulation and experiment). The results obtained demonstrate good agreement with both simple analytic equations and experiment measurements; moreover, simulations were verified independently by using the angular spectrum method [47,48] (to simplify, we do not show it in the paper). The scheme of the non-stretched plate is shown in the inset of Fig. 4(g).

5. COMPARISON OF NUMERICAL SIMULATION RESULTS AND EXPERIMENTAL DATA

The comparison between experimental data and 3D numerical simulations (as well as with theoretical predictions based on the simple constructive interference criteria) is presented in Fig. 4 and demonstrates the displacement of the focus position under zone plate stretching. The experimental data are marked by in yellow (error bar corresponds to the standard deviation; we performed three independent measurements for each point) and numerical results in blue and red lines for different directions. We observed a good agreement between numerical and experimental focal lengths for different radii. The large standard deviations in the experiments can be attributed to the infinite coherence length of our BWO emitter, which results in standing waves between different optical elements (surfaces) of the THz beam path and speckle patters that somewhat distort the collected THz images. Other possible reasons are imperfections of our stretching device that cause fluctuations of the zone plate geometry from one experiment to another. For example, when $\Delta R_n/R_n = 0$, focal length from 3D simulation is $f_{\text{sim}} = 19.36$ mm, and mean value $\overline{f_{\text{exp}}} = 17.6$ mm in the experiments. Therefore, the observed deviation between computational simulation and experimental measurements is near $10 - 11\%$ during the entire stretching process. From our point of view, a mismatch of the numerically predicted and experimentally measured focal length can be explained by the non-ideal character of the experimental input beam and its difference from the perfect plane wave. In both cases, the relative focus change, $\Delta f/f$, monotonically increased very similarly during stretching.

The theoretical focal lengths of the zone plate with a high number of zones can be calculated as

$$f = \frac{R_n^2 - \frac{n^2\lambda^2}{4}}{n\lambda}, \tag{1}$$

where $R_n = 10.304$ mm, $N = 10$ is the number of zone, and λ is the operating wavelength of the input beam. The corresponding results under different applied stretchings are presented in Fig. 4(g) by the green line. This analytical solution can include some mistakes due to the small number of zones in the designed zone plate. For this reason, small disagreements with simulations were observed.

We next theoretically, numerically, and experimentally estimate the influence of the stretching effect on the focal spot dimensions of the obtained zone plate [see Figs. 4(h)–4(i)]. Intensity distribution created by the diffraction-limited lens in the focal spot cross section can be described by using the Airy function [49]

$$I(\rho) = \left(\frac{2J_1(\pi D\rho/\lambda f)}{\pi D\rho/\lambda f}\right)^2, \tag{2}$$

where ρ is the radial coordinate in the focal plane, J_1 is the first-order Bessel function, and D is the lens diameter. For a zone plate with N zones and $D = 2R_n$, in the case of plane wave illumination, one can have a simple approximation for spatial resolution (Rayleigh criterion) [50]:

$$\delta = \frac{\beta\lambda f}{2R_n}, \tag{3}$$

where $\beta = 1.22$ if the number of zones $N = \infty$. For a low number $N \geq 7$, parameter β varies within $\pm 10\%$ from 1.22 [51], which is found to be in good agreement with numerical simulations and experimental results. The focal spot diameter along the oy axis for different zone plate stretchings [at the full-width at half-maximum (FWHM)] is shown in Fig. 4(h). Interestingly, the value of $\delta_\sim$ for different polarizations is close enough to the analytical predictions, whereas the experimental spatial resolution has significant disagreement. We consider that it could be because of imperfections in the THz beam that radiates the analyzed optical element and some incline between the optical element axis and input beam in the xoz plane, which could lead to expansion of the focal spot.

Figure 4(i) presents the depth of field of the analyzed zone plate. From Eq. (2), we obtain

$$\delta z = \pm\beta\left(\frac{f}{2R_n}\right)^2\lambda. \tag{4}$$

$\beta \approx 2$, and δ_z is the distance at which the intensity at the center of the focal spot is reduced by 20%. We observed a good agreement between the experiment and numerical modeling, with only slight deviations. This becomes more critical for higher elongation of a zone plate above 15% [Fig. 4(i)].

6. DISCUSSION

Here, the technique for the SWCNT film deposition on the flexible polymer material is developed. The proposed method opens a way for realization of any required pattern with high precision. It is a perspective for the design and fabrication of tunable optical elements for a variety of applications. For example, such a stretchable zone plate can be applied for THz measurements of waveguides

and fibers aimed at accommodating the THz beam path for samples of different lengths [52]. Another option is to use such a zone plate as a key element of THz imaging systems designed for solving the demanding problems of non-destructive testing of materials [53], quality control in pharmaceutics [54], plant science [55], food science [56], security task [57], etc. In all these applications, the THz images of standoff objects are captured and analyzed, while the distance between the THz imaging system and an object varies in a wide range (from a few centimeters to a few meters); thus, the varifocal THz lenses are in order. A tunable THz zone plate should be judiciously designed to meet the demands of the listed applications, including the working distance, focal point tunability, energy efficiency, field of view, numerical aperture, and spatial resolution. In addition, we have recently developed an optically controlled THz modulator that also relies on stretchable SWCNT and exploits similar operation principles [58]. However, development of such a zone plate or other planar optical elements for some particular THz application and their experimental characterization are out of the scope of this paper; we will address these challenges in our future work.

A similar approach was used in [37], in which a stretchable Fresnel lens based on a vertically aligned CNT inside a polydimethyl-siloxane (PDMS) layer was developed for the visible range. For this zone plate, maximal uniform deformations (radial stretching) of up to 11.4% and a change in the focal point position of up to 24% were demonstrated. In turn, the unique physical properties of our polymer substrate allow us to achieve advanced tunability of the focal length (up to 50%, almost two times higher than in [37]). Finally, our methods of planar optical element fabrication appear to be more technologically reliable and robust, because our SWCNT films are easily transferred onto almost any substrate via the dry-transferring technique. At present, the spatial resolution of direct SWCNT deposition has to provide a high-accuracy pattern with mesoscale dimensions. The optical elements for large-wavelength radiation could be manufactured without significant technological difficulties. It should also be mentioned that the proposed composite (SWCNT/elastomer) is mechanically stable and can withstand at least hundreds of cycles with repetition rates of at least several Hz [43]. These important facts open the way for the design and fabrication of different planar THz optical elements for a variety of applications.

Although the developed zone plate was studied at the particular fixed wavelength of our BWO emitter in this study, it is capable of multispectral operation. In fact, due to the physical operation principle, the zone plate focal length f and free-space wavelength λ are related parameters: $r = \sqrt{n\lambda f + \frac{n^2\lambda^2}{4}}$; here, r is the zone plate radius, and n is a number of zones. In this way, we can point out the two regimes of our stretchable zone plate operation. In the first regime, namely, the varifocal one studied in this paper, we fixed the wavelength, stretched the lens, and changed the focal length. In the second regime—let us call it the multispectral one (it remains to be studied)—the focal length is fixed, while the wavelength varies together with the zone plate stretching, aimed at sustaining the desired fixed focal length. For the multispectral regime, the dependence of variable wavelength on the variable zone plate radius can be defined as $\lambda = \frac{2\sqrt{f^2+r^2}-f}{n}$. We also notice that the relative wavelength tunability of such a system should be close to that of the focal lengths. We postponed detailed theoretical and experimental studies of this multispectral regime to our future work.

The high demand for high-precision compact stretching devices for various applications results in design, experimental, and theoretical investigations of the proposed optical elements. Our paper and earlier similar research [37] showed that the optical element shape distortions caused by imperfections of the stretching device brings some disagreement between the theoretically predicted and measured parameter of the THz beam caustic (focus). For further use of the developed stretchable THz optics, novel stretchable devices should be judiciously designed to guarantee isotropic stretching of the zone plate in lateral directions, sustain coaxial position of this element and the THz beam, eliminate zone plate rotation, and reduce the total dimensions of an optical system. For example, the elastomer could be pulled on the drum (hoop)-like device, where the stretching is realized by the relative displacement of the coaxial drum rims. The use of electrically (or optically) tuned devices [59] is widely considered as an alternative way for managing optical elements. Mainly, these devices are rigid and can be realized in various versions: recently gate-tunable metasurfaces [60], tunable dual-band filters [61], and optical delay lines [62] have been proposed. But flexible voltage-driven elements should also be highlighted, such as flexible modulators for the THz frequency range [63,64]. In our opinion, the SWCNT spectrum can be easily tuned in a wide range by electrochemical gating [65], opening an avenue for two-dimensional (via strain and potential) tuning of the planar optical element. Such elements will be practically applicable.

7. EXPERIMENTAL METHODS

SWCNT films fabrication. Let us explain briefly the deposition CVD method used for SWCNT synthesizing. Ferrocene (98%, Sigma Aldrich) was used as a catalyst precursor, while carbon monoxide (99.99 % Linde gas) acted as a carbon source and carrier gas. Ferrocene saturated vapor was introduced in a hot zone (880°C) of a tubular quartz reactor by a CO stream. The Boudouard reaction ($2\,CO = C + CO_2$), occurring on the surface of formed Fe-based aerosol particles, resulted in the formation of SWCNTs. The minor addition of carbon dioxide (99.995% MGPZ) allows tuning the nanotube properties (e.g., diameter distribution) and governing the process efficiency [66]. The resulting SWCNT films consisted of nearly equilibrium composition: one-third metallic and two-thirds semiconducting SWCNTs.

A Perkin Elmer Lambda 1050 UV-VIS-NIR spectrometer was employed to obtain optical the spectrum of SWCNT film, while a Thermoscientific DXRxi Raman Imaging microscope (wavelength of 532 nm) was used for Raman spectroscopy. Helios PFIB G_4 UXe served for scanning electron microscopy studies. Copper-based zone plates were obtained with an ARGUS fiber laser cutting system (Wuhan Sunic Photoelectricity Equipment Manufacture Co., Ltd).

Continuous-wave THz imaging setup. The homemade THz imaging system, based on the BWO, was applied earlier for THz optical element characterization [67,68] and developed in GPI RAS. It features tunable output frequency (of the order of $\nu = 500 - 700$ GHz for single BWO), linewidth of $\sim 10^{-5}\nu$, power of outer radiation $\sim 10^{-2}$mW, sensitivity $\sim 10^{-5}$V/W, and time response of $\sim 10^{-1}$s (using the Golay cell as a detector). Output frequency $\nu = 0.592$ THz in experiments corresponds

to the local maximum in the BWO emission spectrum. The output THz radiation propagates through the system of lenses and mirrors, modulated by a 22 Hz mechanical chopper. The stretch system [see Fig. 3(a)] is printed with a commercial 3D printer and installed in the THz beam. Ten clamps are made radially to apply uniform radial stretch to the lens. The motion of the clamps is generated by the rotational movement of the micrometer. For intensity readout, the combination of a wide-aperture lens and aperture with diameter $d = 500$ μm is used. The detector is mounted on motorized stages with positioning accuracy of ≤ 2 μm, which guarantees an opportunity to perform a 2D pixel-by-pixel scan of the THz field intensity in the oyz plane, which was chosen as the image plane [see Fig. 3(c)]. Also the adjusting linear translator with a micrometer was used as a detector moving along the ox axis (not shown in the scheme). The BWO provides almost linearly polarized radiation (radiation fraction polarized along oy axis reaches 5/6 by total power), so in simulation, we considered the field distributions from the input wave with linearly polarized radiation in the two perpendicular directions.

THz propagation simulations. For numerical simulation of the field interaction with the Fresnel zone plate, COMSOL Multiphysics Softwave was applied. Namely, the quasi-3D finite-element frequency-domain (FEFD) method was used for modeling the optical element with a rotational symmetry [67,69] with respect to the optical axis (oz). The 2D cross section in cylindrical coordinates ($\mathbf{r}$, z) of the focal spot is the result of the calculation ($\mathbf{r}$ is a radius vector perpendicular to the oz axis). First, the two different simulations of the field distribution process were performed when circularly polarized plane waves of angular momentum $m = 1$ and $m = -1$ were introduced in the simulation volume. These different solutions were coherently added and obtained the focal spot corresponding to the linearly polarized plane wave (used as the excitation field in the experiment). The simulation volume was restricted by the cylindrical perfectly matched layers as the absorbing boundaries [70]. In the simulation process, we implemented a perfect conductor as zone plate material.

8. CONCLUSION

To sum up, for the first time, we demonstrated a novel design of tunable lenses based on planar Fresnel zone plates and operate in the THz spectral range (near $\nu = 0.6$ THz in our experiments). Our technique allows the fabrication of variable-focal-length optical elements comprising integrated SWCNT films of predetermined geometry. Obtained results corroborate the robustness and high efficiency of the designed elements, demonstrating high repeatability for a series of stretching circles. Despite the considered case of operation, when achieving a 50% change in focus length with a 21% increase in the zone plate outer radius, our experimental studies are in good agreement with performed theoretical, both analytical and numerical, evaluations. The presented tunable device may further enable the integration of SWCNT films into photonic and optoelectronic applications. Our approach could be of use for prompting the creation of a variety of flexible and stretchable optical elements in the THz spectral range.

Funding. Ministry of Science and Higher Education of the Russian Federation (075-15-2021-606); Russian Science Foundation (21-79-10097, 22-13-00436, 22-72-10033).

Acknowledgment. G.M.K., D.A.G., and M.G.B. acknowledge the Russian Science Foundation (RSF) project No. 21-79-10097 (numerical investigation of the THz zone plate properties); also, G.M.K. acknowledges the RSF project No. 22-72-10033 (experimental imaging of the THz field). D.A.G., A.V.A, and V.S.V. acknowledge the M. of Science and Higher Education of the Russian Federation Project No. 075-15-2021-606 (design and fabrication of the stretching device). N.I.R. and A.G.N. acknowledge RSF project No. 22-13-00436 (synthesis of single-walled carbon nanotubes).

Disclosures. The authors declare no conflicts of interest.

Data availability. Data underlying the results presented in this paper are not publicly available at this time but may be obtained from the authors upon reasonable request.

REFERENCES

1. S. Lepeshov, A. Gorodetsky, A. Krasnok, E. Rafailov, and P. Belov, "Enhancement of terahertz photoconductive antenna operation by optical nanoantennas," Laser Photon. Rev. **11**, 1600199 (2017).
2. A. E. Yachmenev, D. V. Lavrukhin, I. A. Glinskiy, N. V. Zenchenko, Y. G. Goncharov, I. E. Spektor, R. A. Khabibullin, T. Otsuji, and D. S. Ponomarev, "Metallic and dielectric metasurfaces in photoconductive terahertz devices: a review," Opt. Eng. **59**, 061608 (2019).
3. O. P. Cherkasova, D. S. Serdyukov, E. F. Nemova, A. S. Ratushnyak, A. S. Kucheryavenko, I. N. Dolganova, G. Xu, M. Skorobogatiy, I. V. Reshetov, P. S. Timashev, I. E. Spektor, K. I. Zaytsev, and V. V. Tuchin, "Cellular effects of terahertz waves," J. Biomed. Opt. **26**, 090902 (2021).
4. H. Guerboukha, K. Nallappan, and M. Skorobogatiy, "Toward real-time terahertz imaging," Adv. Opt. Photon. **10**, 843–938 (2018).
5. Y. Zhiyao, Z. Li-Guo, M. Kun, H. Wanxia, and S. Qiwu, "THz medical imaging: from in vitro to in vivo," Trends Biotechnol. **40**, 816–830 (2022).
6. Z. Chen, X. Ma, B. Zhang, Y. Zhang, Z. Niu, N. Kuang, W. Chen, L. Li, and S. Li, "A survey on terahertz communications," China Commun. **16**, 1–35 (2019).
7. M. G. Burdanova, A. P. Tsapenko, M. V. Kharlamova, E. I. Kauppinen, B. P. Gorshunov, J. Kono, and J. Lloyd-Hughes, "A review of the terahertz conductivity and photoconductivity of carbon nanotubes and heteronanotubes," Adv. Opt. Mater. **9**, 2101042 (2021).
8. M. G. Burdanova, A. P. Tsapenko, D. A. Satco, R. Kashtiban, C. D. W. Mosley, M. Monti, M. Staniforth, J. Sloan, Y. G. Gladush, A. G. Nasibulin, and J. Lloyd-Hughes, "Giant negative terahertz photoconductivity in controllably doped carbon nanotube networks," ACS Photon. **6**, 1058–1066 (2019).
9. M. G. Burdanova, M. Liu, M. Staniforth, Y. Zheng, R. Xiang, S. Chiashi, A. Anisimov, E. I. Kauppinen, S. Maruyama, and J. Lloyd-Hughes, "Intertube excitonic coupling in nanotube van der waals heterostructures," Adv. Funct. Mater. **32**, 2104969 (2021).
10. M.-F. Yu, B. S. Files, S. Arepalli, and R. S. Ruoff, "Tensile loading of ropes of single wall carbon nanotubes and their mechanical properties," Phys. Rev. Lett. **84**, 5552–5555 (2000).
11. Q. Zhang, N. Wei, P. Laiho, and E. I. Kauppinen, "Recent developments in single-walled carbon nanotube thin films fabricated by dry floating catalyst chemical vapor deposition," Top. Curr. Chem. **375**, 90 (2017).
12. A. G. Nasibulin, A. Moisala, D. P. Brown, H. Jiang, and E. I. Kauppinen, "A novel aerosol method for single walled carbon nanotube synthesis," Chem. Phys. Lett. **402**, 227–232 (2005).
13. M. Jin, Y. Wang, M. Chai, C. Chen, Z. Zhao, and T. He, "Terahertz detectors based on carbon nanomaterials," Adv. Funct. Mater. **32**, 2107499 (2021).
14. R. R. Hartmann, J. Kono, and M. E. Portnoi, "Terahertz science and technology of carbon nanomaterials," Nanotechnology **25**, 322001 (2014).
15. M. G. Burdanova, G. M. Katyba, R. Kashtiban, G. A. Komandin, E. Butler-Caddle, M. Staniforth, A. A. Mkrtchyan, D. V. Krasnikov, Y. G. Gladush, J. Sloan, A. G. Nasibulin, and J. Lloyd-Hughes, "Ultrafast, high modulation depth terahertz modulators based on carbon nanotube thin films," Carbon **173**, 245–252 (2021).
16. L. Cai and C. Wang, "Carbon nanotube flexible and stretchable electronics," Nano. Res. Lett. **10**, 320 (2015).
17. H. Jang, Y. J. Park, X. Chen, T. Das, M.-S. Kim, and J.-H. Ahn, "Graphene-based flexible and stretchable electronics," Adv. Mater. **28**, 4184–4202 (2016).

18. D. Suzuki and Y. Kawano, "Flexible terahertz imaging systems with single-walled carbon nanotube films," Carbon **162**, 13–24 (2020).
19. S.-T. Xu, L.-L. Mou, F. Fan, S. Chen, Z. Zhao, D. Xiang, M. J. de Andrade, Z. Liu, and S.-J. Chang, "Mechanical modulation of terahertz wave via buckled carbon nanotube sheets," Opt. Express **26**, 28738–28750 (2018).
20. N. Krumbholz, T. Hochrein, N. Vieweg, T. Hasek, K. Kretschmer, M. Bastian, M. Mikulics, and M. Koch, "Monitoring polymeric compounding processes inline with THz time-domain spectroscopy," Polym. Test. **28**, 30–35 (2009).
21. N. V. Chernomyrdin, M. E. Frolov, S. P. Lebedev, I. V. Reshetov, I. E. Spektor, V. L. Tolstoguzov, V. E. Karasik, A. M. Khorokhorov, K. I. Koshelev, A. O. Schadko, S. O. Yurchenko, and K. I. Zaytsev, "Wide-aperture aspherical lens for high-resolution terahertz imaging," Rev. Sci. Instrum. **88**, 014703 (2017).
22. C. Jastrow, K. Münter, R. Piesiewicz, T. Kürner, M. Koch, and T. Kleine-Ostmann, "300 GHz transmission system," Electron. Lett. **44**, 213 (2008).
23. Y. H. Lo and R. Leonhardt, "Aspheric lenses for terahertz imaging," Opt. Express **16**, 15991–15998 (2008).
24. R. Appleby and H. B. Wallace, "Standoff detection of weapons and contraband in the 100 GHz to 1 THz region," IEEE Trans. Antennas Propag. **55**, 2944–2956 (2007).
25. G. C. Knollman, J. L. S. Bellin, and J. L. Weaver, "Variable-focus liquid-filled hydroacoustic lens," J. Acoust. Soc. Am. **49**, 253–261 (1971).
26. A. H. Rawicz and I. Mikhailenko, "Modeling a variable-focus liquid-filled optical lens," Appl. Opt. **35**, 1587–1589 (1996).
27. B. Scherger, C. Jördens, and M. Koch, "Variable-focus terahertz lens," Opt. Express **19**, 4528–4535 (2011).
28. J.-S. Li, "Tunable focus graphene-based terahertz lens," Opt. Commun. **359**, 268–271 (2016).
29. M.-K. Chen, Y.-C. Chang, C.-E. Yang, Y. Guo, J. Mazurowski, S. Yin, P. Ruffin, C. Brantley, E. Edwards, and C. Luo, "Tunable terahertz plasmonic lenses based on semiconductor microslits," Microw. Opt. Technol. Lett. **52**, 979–981 (2010).
30. M. Wichmann, A. S. Mondol, N. Kocic, S. Lippert, T. Probst, M. Schwerdtfeger, S. Schumann, T. Hochrein, P. Heidemeyer, M. Bastian, G. Bastian, and M. Koch, "Terahertz plastic compound lenses," Appl. Opt. **52**, 4186–4191 (2013).
31. S. Indrišiūnas, H. Richter, I. Grigelionis, V. Janonis, L. Minkevičius, G. Valušis, G. Račiukaitis, T. Hagelschuer, H.-W. Hübers, and I. Kašalynas, "Laser-processed diffractive lenses for the frequency range of 4.7 THz," Opt. Lett. **44**, 1210–1213 (2019).
32. A. Siemion, A. Siemion, M. Makowski, J. Suszek, J. Bomba, A. Czerwiński, F. Garet, J.-L. Coutaz, and M. Sypek, "Diffractive paper lens for terahertz optics," Opt. Lett. **37**, 4320–4322 (2012).
33. V. Pavelyev, M. Komlenok, B. Volodkin, B. Knyazev, T. Kononenko, V. Konov, V. Soifer, and Y. Choporova, "Fabrication of high-effective silicon diffractive optics for the terahertz range by femtosecond laser ablation," Phys. Procedia **84**, 170–174 (2016).
34. S. Al-Daffaie, A. J. Jumaah, V. L. Rubio, and T. Kusserow, "Design and implementation of a terahertz lens-antenna for a photonic integrated circuits based THz systems," Sci. Rep. **12**, 1476 (2022).
35. M. I. B. Shams, Z. Jiang, S. M. Rahman, L.-J. Cheng, J. L. Hesler, P. Fay, and L. Liu, "A 740 GHz dynamic two-dimensional beam-steering and forming antenna based on photo-induced reconfigurable Fresnel zone plates," IEEE Trans. Terahertz Sci. Technol. **7**, 310–319 (2017).
36. E. Minerbi, S. Keren-Zur, and T. Ellenbogen, "Nonlinear metasurface Fresnel zone plates for terahertz generation and manipulation," Nano Lett. **19**, 6072–6077 (2019).
37. X. Li, L. Wei, R. H. Poelma, S. Vollebregt, J. Wei, H. P. Urbach, P. M. Sarro, and G. Q. Zhang, "Stretchable binary Fresnel lens for focus tuning," Sci. Rep. **6**, 25348 (2016).
38. X. Xia, Y. Li, F. Cai, H. Zhou, T. Ma, and H. Zheng, "Ultrasonic tunable focusing by a stretchable phase-reversal Fresnel zone plate," Appl. Phys. Lett. **117**, 021904 (2020).
39. E. M. Khabushev, D. V. Krasnikov, O. T. Zaremba, A. P. Tsapenko, A. E. Goldt, and A. G. Nasibulin, "Machine learning for tailoring optoelectronic properties of single-walled carbon nanotube films," J. Phys. Chem. Lett. **10**, 6962–6966 (2019).
40. A. Kaskela, A. G. Nasibulin, M. Y. Timmermans, B. Aitchison, A. Papadimitratos, Y. Tian, Z. Zhu, H. Jiang, D. P. Brown, A. Zakhidov, and E. I. Kauppinen, "Aerosol-synthesized SWCNT networks with tunable conductivity and transparency by a dry transfer technique," Nano Lett. **10**, 4349–4355 (2010).
41. H. Kataura, Y. Kumazawa, Y. Maniwa, I. Umezu, S. Suzuki, Y. Ohtsuka, and Y. Achiba, "Optical properties of single-wall carbon nanotubes," Synth. Met. **103**, 2555–2558 (1999).
42. P. Eklund, J. Holden, and R. Jishi, "Vibrational modes of carbon nanotubes; spectroscopy and theory," Carbon **33**, 959–972 (1995).
43. E. P. Gilshteyn, S. A. Romanov, D. S. Kopylova, G. V. Savostyanov, A. S. Anisimov, O. E. Glukhova, and A. G. Nasibulin, "Mechanically tunable single-walled carbon nanotube films as a universal material for transparent and stretchable electronics," ACS Appl. Mater. Interfaces **11**, 27327–27334 (2019).
44. H. Quinn and M. Thomas, "Device for cell culture on deformable surfaces," U.S. patent 7,807,453 B2 (October 5, 2010).
45. G. A. Komandin, S. V. Chuchupal, S. P. Lebedev, Y. G. Goncharov, A. F. Korolev, O. E. Porodinkov, I. E. Spektor, and A. A. Volkov, "BWO generators for terahertz dielectric measurements," IEEE Trans. Terahertz Sci. Technol. **3**, 440–444 (2013).
46. F. A. Jenkins and H. E. White, *Fundamentals of Optics*, 4th ed. (McGraw-Hili Primls Custom Publishing, 1976).
47. N. V. Petrov, M. S. Kulya, A. N. Tsypkin, V. G. Bespalov, and A. Gorodetsky, "Application of terahertz pulse time-domain holography for phase imaging," IEEE Trans. Terahertz Sci. Technol. **6**, 464–472 (2016).
48. A. T. Turov, M. S. Kulya, N. V. Petrov, and A. Gorodetsky, "Resolution and contrast in terahertz pulse time-domain holographic reconstruction," Appl. Opt. **58**, G231–G240 (2019).
49. M. Born and E. Wolf, *Principles of Optics: Electromagnetic Theory of Propagation, Interference and Diffraction of Light*, 7th ed. (Cambridge University, 1999).
50. J. Kirz and D. Attwood, "Zone plates," in *X-Ray Data Booklet* (University of California, 2009).
51. M. Sussman, "Elementary diffraction theory of zone plates," Am. J. Phys **28**, 394–398 (1960).
52. G. Katyba, K. Zaytsev, N. Chernomyrdin, I. Shikunova, G. Komandin, V. Anzin, S. Lebedev, I. Spektor, V. Karasik, S. Yurchenko, I. Reshetov, V. Kurlov, and M. Skorobogatiy, "Sapphire photonic crystal waveguides for terahertz sensing in aggressive environments," Adv. Opt. Mater. **6**, 1800573 (2018).
53. C. D. Stoik, M. J. Bohn, and J. L. Blackshire, "Nondestructive evaluation of aircraft composites using transmissive terahertz time domain spectroscopy," Opt. Express **16**, 17039–17051 (2008).
54. J. A. Zeitler, P. F. Taday, D. A. Newnham, M. Pepper, K. C. Gordon, and T. Rades, "Terahertz pulsed spectroscopy and imaging in the pharmaceutical setting—a review," J. Pharm. Pharmacol. **59**, 209–223 (2007).
55. A. V. Shchepetilnikov, A. M. Zarezin, V. M. Muravev, P. A. Gusikhin, and I. V. Kukushkin, "Quantitative analysis of water content and distribution in plants using terahertz imaging," Opt. Eng. **59**, 061617 (2020).
56. N. V. Penkov, M. V. Goltyaev, M. E. Astashev, D. A. Serov, M. N. Moskovskiy, D. O. Khort, and S. V. Gudkov, "The application of terahertz time-domain spectroscopy to identification of potato late blight and fusariosis," Pathogens **10**, 1336 (2021).
57. I. N. Dolganova, K. I. Zaytsev, S. O. Yurchenko, V. E. Karasik, and V. V. Tuchin, "The role of scattering in quasi-ordered structures for terahertz imaging: local order can increase an image quality," IEEE Trans. Terahertz Sci. Technol. **8**, 403–409 (2018).
58. M. I. Paukov, V. V. Starchenko, D. V. Krasnikov, G. A. Komandin, Y. G. Gladush, S. S. Zhukov, B. P. Gorshunov, A. G. Nasibulin, A. V. Arsenin, V. S. Volkov, and M. G. Burdanova, "Ultrafast opto-mechanical terahertz modulators based on stretchable carbon nanotube thin films," arXiv arXiv:2211.07312 (2022).
59. Z. T. Ma, Z. X. Geng, Z. Y. Fan, J. Liu, and H. D. Chen, "Modulators for terahertz communication: the current state of the art," Research **2019**, 6482975 (2019).
60. Y.-W. Huang, H. W. H. Lee, R. Sokhoyan, R. A. Pala, K. Thyagarajan, S. Han, D. P. Tsai, and H. A. Atwater, "Gate-tunable conducting oxide metasurfaces," Nano Lett. **16**, 5319–5325 (2016).
61. W. Feng, Y. Zhang, and W. Che, "Tunable dual-band filter and diplexer based on folded open loop ring resonators," IEEE Trans. Circuits Syst. II Express Briefs **64**, 1047–1051 (2017).

62. T. Tatoli, D. Conteduca, F. Dell'Olio, C. Ciminelli, and M. N. Armenise, "Graphene-based fine-tunable optical delay line for optical beam-forming in phased-array antennas," Appl. Opt. **55**, 4342–4349 (2016).
63. D.-Y. Khang, H. Jiang, Y. Huang, and J. A. Rogers, "A stretchable form of single-crystal silicon for high-performance electronics on rubber substrates," Science **311**, 208–212 (2006).
64. K. Fan, X. Zhao, J. Zhang, K. Geng, G. R. Keiser, H. R. Seren, G. D. Metcalfe, M. Wraback, X. Zhang, and R. D. Averitt, "Optically tunable terahertz metamaterials on highly flexible substrates," IEEE Trans. Terahertz Sci. Technol. **3**, 702–708 (2013).
65. D. S. Kopylova, D. A. Satco, E. M. Khabushev, A. V. Bubis, D. V. Krasnikov, T. Kallio, and A. G. Nasibulin, "Electrochemical enhancement of optoelectronic performance of transparent and conducting single-walled carbon nanotube films," Carbon **167**, 244–248 (2020).
66. E. M. Khabushev, D. V. Krasnikov, J. V. Kolodiazhnaia, A. V. Bubis, and A. G. Nasibulin, "Structure-dependent performance of single-walled carbon nanotube films in transparent and conductive applications," Carbon **161**, 712–717 (2020).
67. V. E. Ulitko, G. M. Katyba, V. A. Zhelnov, I. M. Shmytko, G. A. Emelchenko, I. E. Spector, V. M. Masalov, V. N. Kurlov, K. I. Zaytsev, and M. Skorobogatiy, "Opal-based terahertz optical elements fabricated by self-assembly of porous SiO_2 nanoparticles," Opt. Express **29**, 13764–13777 (2021).
68. K. Zaytsev, G. Katyba, N. Chernomyrdin, I. Dolganova, A. Kucheryavenko, A. Rossolenko, V. Tuchin, V. Kurlov, and M. Skorobogatiy, "Overcoming the ABBE diffraction limit using a bundle of metal-coated high-refractive-index sapphire optical fibers," Adv. Opt. Mater. **8**, 2000307 (2020).
69. M. Albani and P. Bernardi, "A numerical method based on the discretization of maxwell equations in integral form (Short Papers)," IEEE Trans. Microwave Theory Tech. **22**, 446–450 (1974).
70. J. B. Schneider, *Understanding the Finite-Difference Time-Domain Method* (Springer, 2010).